RSC Advances

PAPER

View Article Online
View Journal | View Issue

Open Access Article. Published on 02 January 2018. Downloaded on 5/23/2026 9:34:01 PM.
This article is licensed under a Creative Commons Attribution 3.0 Unported Licence.

Check for updates

Cite this: *RSC Adv.*, 2018, **8**, 302

Valence of Ti cations and its effect on magnetic properties of spinel ferrites $Ti_xM_{1-x}Fe_2O_4$ (M = Co, Mn)

Y. N. Du,[a] J. Xu,[ab] Z. Z. Li,[a] G. D. Tang,*[ac] J. J. Qian,[a] M. Y. Chen[a] and W. H. Qi[a]

Received 6th November 2017
Accepted 13th December 2017

DOI: 10.1039/c7ra12163f

rsc.li/rsc-advances

Powder samples of $Ti_xCo_{1-x}Fe_2O_4$ ($0.0 \le x \le 0.4$) and $Ti_xMn_{1-x}Fe_2O_4$ ($0.0 \le x \le 0.3$) were synthesized using a conventional method for preparing ceramics. X-ray diffraction analysis confirmed that the samples consisted of a single phase with a cubic $(A)[B]_2O_4$ spinel structure. The average molecular magnetic moment (μ_{exp}) measured at 10 K decreased monotonically with increasing x for two series of samples. According to previous investigations, Ti^{2+} and Ti^{3+} cations are present in these ferrites, but there are no Ti^{4+} cations; the magnetic moments of the Ti^{2+}, Ti^{3+}, and Mn^{3+} cations are assumed to couple antiferromagnetically with those of the Mn^{2+}, Co^{2+}, Co^{3+}, Fe^{2+}, and Fe^{3+} cations whenever they are at the (A) or [B] sublattice. The dependence of μ_{exp} of the two series of samples on the doping level x was fitted using a quantum-mechanical potential barrier, and the cation distributions in the two series of samples were obtained.

1 Introduction

Spinel ferrites have received much attention in recent years because of their application in spintronics and multiferroics.[1–7] In a $(A)[B]_2O_4$ spinel ferrite, each unit cell contains eight formula units, in which the 32 larger oxygen anions form a close-packed face-centered-cubic structure with the 24 smaller metal cations occupying two types of interstitial position: the tetrahedral (8a) or (A) sites and the octahedral (16d) or [B] sites,[8–11] which form the (A) and [B] sublattices.

Many studies were carried out on the magnetic moment of and cation distribution in Ti-doped spinel ferrites.[12–16] In these investigations, all of the Ti cations were assumed to be tetravalent, but there have been disputes regarding the cation distribution. Dwivedi *et al.* prepared a series of samples, $Co(Fe_{1-x}Ti_x)_2O_4$ (x = 0, 0.05, or 0.1), by conventional solid-phase reactions; using X-ray photoelectron spectroscopy (XPS) they discovered that all Ti cations went into the octahedral sites.[12] Srinivasa Rao *et al.* prepared samples of the $CoTi_xFe_{2-x}O_4$ ($0.0 \le x \le 0.3$) series; they thought that the Ti^{4+} ions had the tendency to go to the [B] site, which affected the cation distribution in the samples.[13] Schmidbauer prepared samples of the $Fe_{1+x}Cr_{2-2x}Ti_xO_4$ ($0 \le x \le 1$) series and concluded that there were Fe^{2+} ions at the (A) and [B] sites, and all Cr and Ti cations occupied the B-sites.[14] Schmidbauer also prepared samples of two spinel ferrite series, $Fe_{2.4-t}Cr_{0.6}Ti_tO_4$ ($0 \le t \le 0.7$) and $Fe_{2.1-t}Cr_{0.9}Ti_tO_4$ ($0 \le t \le 0.55$), and assumed that all of the Ti^{4+} ions entered the [B] sites.[15] However, when Kale *et al.* prepared $Ti_xNi_{1+x}Fe_{2-2x}O_4$ ($0.0 \le x \le 0.7$), they estimated the cation distribution at the (A) and [B] sites using X-ray diffraction and came to the conclusion that the fraction of Ti^{4+} cations entering the (A) sites increased with increasing x, and it reached 0.5 when $x = 0.7$.[16]

In order to resolve these discrepancies regarding cation distributions in spinel ferrites, Xu *et al.* investigated the valence, distribution of cations and the magnetic structure of Ti-doped spinel ferrites[17–19] by using an O 2p itinerant-electron model.[20–22] They found an additional antiferromagnetic phase when Ti cations replaced a portion of the Ni or Fe cations in the spinel ferrites $Ni_{0.68}Fe_{2.32}O_4$ (ref. 17 and 18) and $NiFe_2O_4$,[19] and they offered the following explanation for the phenomenon: most of the Ti cations were Ti^{2+} cations that occupied the [B] sites; the remaining Ti cations were Ti^{3+} cations and there were no Ti^{4+} cations; the magnetic moments of the Ti cations coupled antiferromagnetically with those of Fe and Ni cations whenever they were at the (A) or [B] sites.

The absence of Ti^{4+} in an oxide has been confirmed by theoretical and experimental investigations. Cohen[23] and Cohen and Krakauer[24] used density functional theory to calculate the densities of states for valence electrons in the perovskite oxide $BaTiO_3$. Their results indicated that the average valence of Ba is +2, which is the same as the traditionally accepted value, but the average valences of Ti and O are +2.89 and −1.63,

[a]Hebei Advanced Thin Film Laboratory, Department of Physics, Hebei Normal University, Shijiazhuang City 050024, People's Republic of China. E-mail: tanggd@hebtu.edu.cn; Tel: +86 311 80787330

[b]School of Science, Hebei University of Engineering, Handan City, 050038, People's Republic of China

[c]State Key Laboratory of Magnetism, Institute of Physics, Chinese Academy of Sciences, Beijing 100190, People's Republic of China

This journal is © The Royal Society of Chemistry 2018

Open Access Article. Published on 02 January 2018. Downloaded on 5/23/2026 9:34:01 PM.
This article is licensed under a Creative Commons Attribution 3.0 Unported Licence.

respectively, which are different from the conventional results of +4 and −2, respectively. This calculation result was confirmed by the X-ray photoelectron spectra obtained by Wu *et al.*,[25] who found that the average valence of O anions, V_{alO}, is −1.55, which is close to the value (−1.63) calculated by Cohen. In addition, using XPS analysis, Dupin *et al.* found that the average valence of O anions is −1.15 for TiO_2,[26] which indicates that there are Ti^{2+} and Ti^{3+} cations, but no Ti^{4+} cations, in TiO_2. Ji *et al.* proposed a method to estimate the valences of cations and anions in $(A)[B]_2O_4$ spinel ferrites; they obtained estimated values between −1.6 and −1.8 for V_{alO} of spinel ferrites, and they also defined the ionicity of an oxide as $f_i = |V_{alO}|/2$, accompanied by calculated values of the iconicity of several cations in spinel ferrites.[27]

Taking into account that there are O^{1-} ions in addition to O^{2-} ions, our group uses the O 2p itinerant-electron model[20] and the quantum mechanical potential barrier method[21,22] to investigate the cation distribution in several series of spinel ferrites.[28–35] In the study reported here, we prepared spinel ferrite samples of $Ti_xCo_{1-x}Fe_2O_4$ ($0.0 \le x \le 0.4$) and $Ti_xMn_{1-x}Fe_2O_4$ ($0.0 \le x \le 0.3$) and measured the magnetic moment, μ_{exp}, of the samples at 10 K. The cation distribution in the samples was estimated by fitting the measured values of μ_{exp}.

2 Experimental

2.1 Sample preparation

Spinel ferrites $Ti_xCo_{1-x}Fe_2O_4$ ($0.0 \le x \le 0.4$; hereafter referred to as the Co-series) and $Ti_xMn_{1-x}Fe_2O_4$ ($0.0 \le x \le 0.3$; hereafter referred to as the Mn-series) were prepared using the method of solid-phase reaction.[17] The analytical reagent (AR)-grade chemicals CoO, MnO_2, Fe_2O_3, and TiO_2 were used as the starting materials. First, stoichiometric amounts of each chemical were mixed together, ground for 8 h in an agate mortar, and then calcined at 1173 K for 5 h. The calcined materials were then ground again for 1 h. The ground powder was calcined at 1473 K for an additional 5 h, and then further ground for 1 h. Next, the twice calcined and thrice ground powder was pressed into pellets at a pressure of 10^4 kg cm^{-2} and then sintered at 1673 K for 10 h in a tube furnace under an argon flow. The sintered pellets were then ground for 30 min in an agate mortar, and the resulting powder was used for the measurements.

2.2 Sample characterization

The crystal structure of the samples was determined by analyzing their X-ray diffraction (XRD) patterns, which were measured with an X-ray diffractometer (X'pert Pro, PANalytical, The Netherlands) with Cu K_α ($\lambda = 1.5406$ Å) radiation at room temperature. The data were collected in the 2θ range of 15–120° with a step size of 0.0167°. The working current and voltage were 40 mA and 40 kV, respectively. The magnetic hysteresis loops of the samples were measured using a physical properties measurement system (PPMS, Quantum Design Corporation, USA) at 10 and 300 K.

3 Experimental results

3.1 Analysis of X-ray diffraction patterns

Fig. 1(a) and (b) show the XRD patterns of the $Ti_xCo_{1-x}Fe_2O_4$ ($0.0 \le x \le 0.4$) and $Ti_xMn_{1-x}Fe_2O_4$ ($0.0 \le x \le 0.3$) samples, which indicate that they consisted of a single-phase with a cubic spinel structure of space group $Fd\bar{3}m$. The XRD data were fitted using the X'Pert HighScore Plus software (PANalytical, The Netherlands) and the Rietveld powder-diffraction profile-fitting technique.[36] The ions O (32e), A (8b) and B (16c) were located at the positions (u, u, u), (0.375, 0.375, 0.375), and (0, 0, 0), respectively. We obtained the crystal structure data, including the crystal lattice constant, a, the oxygen position parameters, u, the distances from the O anions to the cations at the (A) and [B] sites, d_{AO} and d_{BO}; and the distance between the cations at the (A) sites and those at the [B] sites, d_{AB}; the data are summarized in Table 1. For the cubic spinel structure, the ideal values (assuming $u = 0.25$) of d_{AO}, d_{BO}, and d_{AB} are $\sqrt{3}a/8$, $a/4$, and $\sqrt{11}a/8$, respectively; however, the observed values of d_{AO} and d_{BO} (Table 1) are 1.0400 and 0.9805 (or 1.0918 and 0.9565) times, respectively, of the ideal values for the Co-series (or Mn-series) samples. On the other hand, the observed values of d_{AB} are equal to the ideal values for the two series. The volume-averaged crystallite sizes of all samples were calculated using

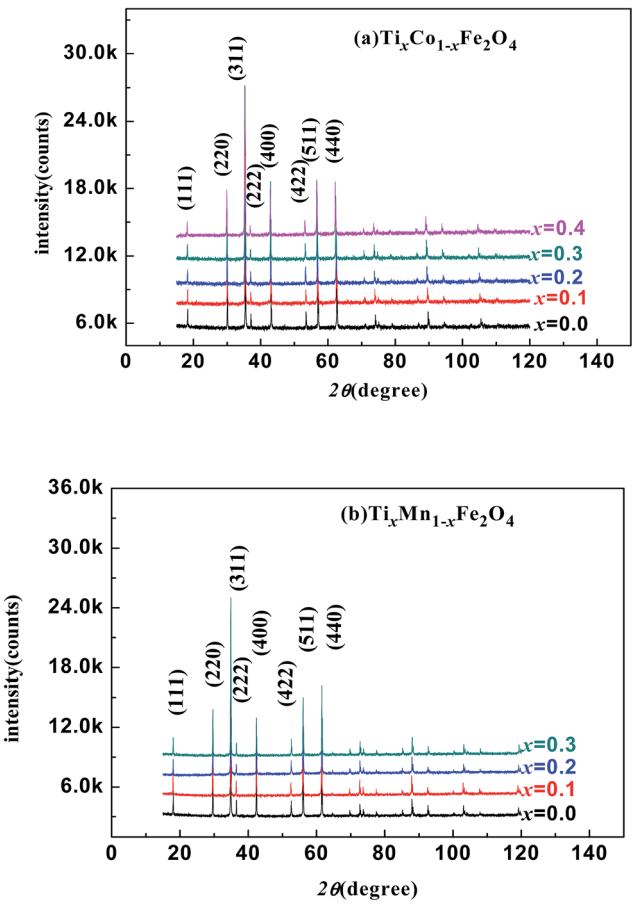

Fig. 1 X-ray diffraction patterns of various samples: (a) $Ti_xCo_{1-x}Fe_2O_4$ ($0.0 \le x \le 0.4$); (b) $Ti_xMn_{1-x}Fe_2O_4$ ($0.0 \le x \le 0.3$).

Open Access Article. Published on 02 January 2018. Downloaded on 5/23/2026 9:34:01 PM.
This article is licensed under a Creative Commons Attribution 3.0 Unported Licence.

Table 1 Rietveld fitting results of XRD patterns of the two series of samples, obtained using the X'Pert HighScore Plus software. a is the lattice parameter; d_{AO} and d_{BO} are the distances from the O anion to the cations at the (A) and [B] sites, respectively; and d_{AB} is the distance from the cations at the (A) sites to those at the [B] sites

x	a (Å)	d_{AO} (Å)	d_{BO} (Å)	d_{AB} (Å)	u (Å)
$Ti_xCo_{1-x}Fe_2O_4$					
0.0	8.3871	1.888	2.056	3.477	0.24503
0.1	8.3987	1.891	2.059	3.482	0.24501
0.2	8.4089	1.893	2.061	3.486	0.24500
0.3	8.4203	1.896	2.064	3.491	0.24499
0.4	8.4343	1.898	2.066	3.497	0.24498
$Ti_xMn_{1-x}Fe_2O_4$					
0.0	8.5197	2.014	2.037	3.532	0.23856
0.1	8.5190	2.016	2.038	3.531	0.23857
0.2	8.5172	2.012	2.036	3.530	0.23858
0.3	8.5118	2.011	2.035	3.529	0.23859

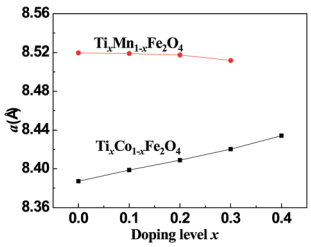

Fig. 2 Curves of lattice constant, a, *versus* the Ti-doping level, x, for the two series of samples.

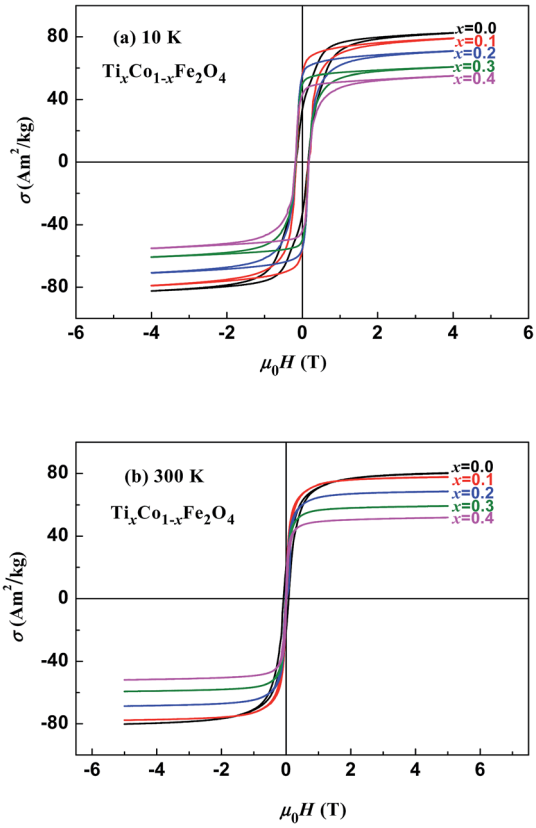

Fig. 3 Magnetic hysteresis loops measured at (a) 10 K and (b) 300 K for samples of $Ti_xCo_{1-x}Fe_2O_4$.

the X'Pert HighScore Plus software, and they were found to be greater than 100 nm. Therefore, surface effects of the crystallites are expected to be very weak in all samples.

Fig. 2 shows the dependence of the lattice parameter a on the Ti-doping level, x, in the two series of samples. It can be seen that with increasing x, a increased for the Co-series and decreased for the Mn-series. The different trends in the lattice constant were related to the cation radii, magnetic ordering, and cohesive energies of the samples.

3.2 Analysis of magnetic properties of the samples

Fig. 3 and 4 show the magnetic hysteresis loops of the two series of samples measured at 10 and 300 K. From these figures, we obtained the specific saturation magnetization (σ_S) measured at 10 and 300 K and the magnetic moment (μ_{exp}) per formula unit of each sample at 10 K, as listed in Table 2. It can be seen that the values of σ_S for the two series of samples gradually decreased with increasing x at both 10 and 300 K.

4 Estimation of cation distributions by fitting the samples' magnetic moments at 10 K

Following the procedure reported by Xu *et al.*,[18–20] we used the O 2p itinerant-electron model[20] and the quantum mechanical potential barrier method[21,22] to fit the magnetic moments measured at 10 K as a function of x and estimate the cation distribution in all samples. During the fitting process, the following factors were taken into account:

Factor 1: since there were O^{1-} ions in addition to O^{2-} ions, the ionicity of the cations in the samples was distinctly lower than 1.0, as shown in Table 3; the values listed in Table 3 were calculated using the method reported by Ji *et al.*[27] In $(A)[B]_2O_4$ spinel ferrites, the total valence and the total number of trivalent cations per formula unit (N_3) are both less than the traditional values of 8 and 2, respectively.

Factor 2: the O 2p itinerant-electron model is characterized by certain features:[20] (i) in a given sublattice, an O 2p electron with constant spin direction can hop from an O^{2-} anion to the O 2p hole of an adjacent O^{1-} anion, with a cation acting as an intermediary. (ii) The two O 2p electrons in the outer orbit of an O^{2-} anion, which have opposite spin directions, become itinerant electrons in the two different sublattices (the (A) or [B] sublattice). (iii) In a given sublattice that is constrained by Hund's rules and by the fact that an itinerant electron has constant spin direction, the direction of the magnetic moments of cations with the 3d electron number of $n_d \leq 4$ will couple antiferromagnetically to those of the cations with $n_d \geq 5$ at either the (A) sites or the [B] sites of a spinel ferrite. Therefore, the directions of the magnetic moments of $Ti^{3+}(3d^1)$, $Ti^{2+}(3d^2)$, and $Mn^{3+}(3d^4)$ were antiparallel to those of the magnetic

Open Access Article. Published on 02 January 2018. Downloaded on 5/23/2026 9:34:01 PM.
This article is licensed under a Creative Commons Attribution 3.0 Unported Licence.

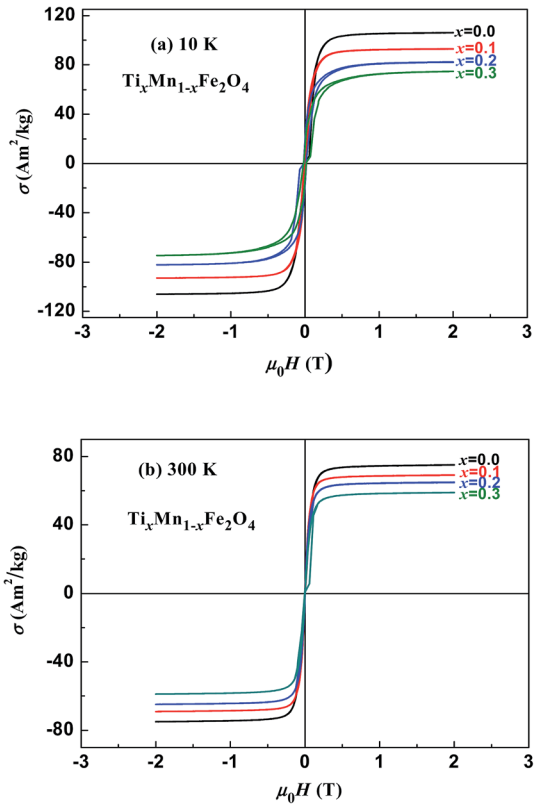

Fig. 4 Magnetic hysteresis loops measured at (a) 10 K and (b) 300 K for samples of $Ti_xMn_{1-x}Fe_2O_4$.

Table 2 Specific saturation magnetization measured at 10 K ($\sigma_{S\text{-}10\ K}$) and 300 K ($\sigma_{S\text{-}300\ K}$) for the two series of samples; μ_{exp} is the experimental magnetic moment per formula unit of a sample, which was calculated using $\sigma_{S\text{-}10K}$

x	$\sigma_{S\text{-}10\ K}$ (A m^2 kg^{-1})	$\sigma_{S\text{-}300\ K}$ (A m^2 kg^{-1})	μ_{exp} (μ_B per formula)
$Ti_xCo_{1-x}Fe_2O_4$			
0.0	77.73	77.39	3.266
0.1	74.19	76.32	3.102
0.2	66.30	67.34	2.759
0.3	59.97	58.03	2.484
0.4	51.02	50.12	2.103
$Ti_xMn_{1-x}Fe_2O_4$			
0.0	105.23	74.41	4.346
0.1	92.28	68.47	3.799
0.2	81.06	64.31	3.327
0.3	72.91	58.18	2.983

moments of Mn^{2+}, Co^{2+}, Co^{3+}, Fe^{3+}, and Fe^{2+} in the same sample at either the (A) sublattice or the [B] sublattice. Therefore, in the following calculations, we set the moment of the cations to the values shown in Table 3.

Factor 3: we assumed that there is a square potential barrier between a pair of anion and cation.[21] The height and the width of the potential barrier are related to the cation ionization energy and the distance between the cation–anion pair. The content ratio (R) of the different cations is therefore related to

Table 3 Cation parameters used in the magnetic-moment fitting process, including the second and third ionization energies, $V(M^{2+})$ and $V(M^{3+})$; effective radii, r, of the divalent cations with coordination number 6; ionicity, f_i;[27] and the magnetic moments of the divalent and trivalent cations, m_2 and m_3

Element, M	$V(M^{2+})$ (eV)	$V(M^{3+})$ (eV)	r^{37} (nm)	f_i^{27}	m_2 (μ_B)	m_3 (μ_B)
Ti	13.58	27.49	0.0860	0.9716	−1	−2
Mn	15.64	33.67	0.0830	0.8293	5	−4
Fe	16.18	30.65	0.0780	0.8790	4	5
Co	17.06	33.50	0.0745	0.8314	3	4

the probability of the last ionized electrons transmitted through the potential barriers, and the following equation can be obtained:

$$R = \frac{P_C}{P_D} = \frac{V_D}{V_C} \exp\left[10.24\left(r_D V_D{}^{1/2} - c r_C V_D{}^{1/2}\right)\right], \quad (1)$$

where nanometers (nm) and electron-volts (eV) are used as the units of length and energy; P_C (or P_D) stands for the probability of the last ionized electron of the C (or D) cation jumping to the anions through the potential barrier with the height V_C (or V_D) and the width r_C (or r_D). V_C and V_D are the ionization energies of the last ionized electron of the cations C and D, and r_C and r_D are the distances from the cations C and D to the anions. The parameter c is a barrier shape-correcting constant related to the different extents to which the shapes of the two potential barriers deviate from a square barrier. When $V_C = V_D$ and $r_C = r_D$, it is obvious that $c = 1.0$.

Factor 4: we considered the Pauli repulsion energy of the electron cloud between adjacent cations and anions. This can be taken into account using the effective ionic radius:[37] smaller ions tend to enter the sites with smaller available space in the lattice. It is worth noting that the volumes of the (A) sites are smaller than those of the [B] sites in spinel ferrites.

Factor 5: during the thermal treatment of the samples, the tendency to balance the electrical charge density forced some of the divalent cations (with large effective ionic radii) to enter the (A) sites (with smaller available space) from the [B] sites (with large available space), jumping over an equivalent potential barrier, V_{BA}, because cations at the (A) sites have four adjacent oxygen ions while cations at the [B] sites have six adjacent oxygen ions. V_{BA} is related to the ionization energy, ionic radius, and the thermal-treatment temperature. We assumed V_{BA} of the ferrite samples can be expressed by the following equations:[34]

$$V_{BA}(Fe^{2+}) = \frac{V_{BA}(Ti^{2+})V(Fe^{3+})r(Fe^{2+})}{V(Ti^{3+})r(Ti^{2+})}, \quad (2)$$

$$V_{BA}(M^{2+}) = \frac{V_{BA}(Ti^{2+})V(M^{3+})r(M^{2+})}{V(Ti^{3+})r(Ti^{2+})}. \quad (3)$$

where M = Co or Mn; $V(M^{3+})$, $V(Ti^{3+})$, and $V(Fe^{3+})$ are the third ionization energies of Co, Mn, Ti and Fe, respectively; and $r(M^{2+})$, $r(Ti^{2+})$, and $r(Fe^{2+})$ are the effective radii of the divalent cations with coordination number 6, as shown in Table 3.

Open Access Article. Published on 02 January 2018. Downloaded on 5/23/2026 9:34:01 PM.
This article is licensed under a Creative Commons Attribution 3.0 Unported Licence.

The chemical formulae of the ferrite samples $Ti_xCo_{1-x}Fe_2O_4$ and $Ti_xMn_{1-x}Fe_2O_4$, are rewritten here as $Ti_{x_1}M_{x_2}Fe_{3-x_1-x_2}O_4$ (M = Co, Mn) so that the cation distributions can be described by the equation

$$(Ti_{y_1}{}^{3+}M_{y_2}{}^{3+}Fe_{y_3}{}^{3+}Ti_{y_4}{}^{2+}M_{y_5}{}^{2+}Fe_{y_6}{}^{2+})[Ti_{x_1-y_1-y_4-z_1}{}^{2+}M_{x_2-y_2-y_5-z_2}{}^{2+}Fe_{3-x_1-x_2-y_3-y_6-z_3}{}^{2+}Ti_{z_1}{}^{3+}M_{z_2}{}^{3+}Fe_{z_3}{}^{3+}]O_4. \quad (4)$$

It can be seen from eqn (4) that

$$y_1 + y_2 + y_3 + y_4 + y_5 + y_6 = 1, \quad (5)$$

$$y_1 + y_2 + y_3 + z_1 + z_2 + z_3 = N_3, \quad (6)$$

$$N_3 = \frac{8}{3}[f_{Ti}x_1 + f_M x_2 + f_{Fe}(3.0 - x_1 - x_2)] - 6.0, \quad (7)$$

where N_3 is the number of trivalent cations per formula unit. The parameters f_{Ti}, f_{Fe}, and $f_M = f_{Co}$ (or f_{Mn}) represent the ionicities of the Ti, Fe, and Co (or Mn) ions,[27] whose values are shown in Table 3. Eqn (7) suggests that when the ionicity of all cations are 1.00, the sum of the valence of all cations is 8.00, while $N_3 = 2.00$. In fact, the ionicity of each cation is lower than 1.00 (see Table 3), resulting in $N_3 < 2.00$. From eqn (4), we have

$$R_{A1}\frac{x_1}{3-x_1-x_2} = \frac{y_1}{y_3},\ R_{A2}\frac{x_2}{3-x_1-x_2} = \frac{y_2}{y_3},\ R_{A4}\frac{x_1}{3-x_1-x_2} = \frac{y_4}{y_3},\ R_{A5}\frac{x_2}{3-x_1-x_2} = \frac{y_5}{y_3},\ R_{A6} = \frac{y_6}{y_3}, \quad (8)$$

$$R_{B1}\frac{x_1-y_1-y_4}{3-x_1-x_2-y_3-y_6} = \frac{z_1}{z_3},\ R_{B2}\frac{x_2-y_2-y_5}{3-x_1-x_2-y_3-y_6} = \frac{z_2}{z_3}, \quad (9)$$

where R_{A1}, R_{A2}, R_{A4}, R_{A5}, and R_{A6} represent the probability ratios of the Ti^{3+}, $Co^{3+}(Mn^{3+})$, Ti^{2+}, $Co^{2+}(Mn^{2+})$, and Fe^{2+} ions, respectively, with respect to the Fe^{3+} ions at the (A) sites, while R_{B1} and R_{B2} represent the probability ratios of the Ti^{3+} and $Co^{3+}(Mn^{3+})$ ions with respect to the Fe^{3+} ions at the [B] sites. From eqn (5) and (8), we can obtain

$$y_3 = \frac{3-x_1-x_2}{(R_{A1}+R_{A4})x_1 + (R_{A2}+R_{A5})x_2 + (1+R_{A6})(3-x_1-x_2)}. \quad (10)$$

From eqn (6) and (9), we have

$$z_3 = \frac{N_3 - \left[1 + R_{A1}\frac{x_1}{3-x_1-x_2} + R_{A2}\frac{x_2}{3-x_1-x_2}\right]y_3}{1 + R_{B1}\frac{x_1-y_1-y_4}{3-x_1-x_2-y_3-y_6} + R_{B2}\frac{x_2-y_2-y_5}{3-x_1-x_2-y_3-y_6}}. \quad (11)$$

According to the above-mentioned quantum mechanical potential barrier method for estimating the cation distributions in spinel ferrites,[21,22] which is similar to eqn (1), the content ratios R_{A1}, R_{A2}, R_{A4}, R_{A5}, and R_{A6} at the (A) sites and R_{B1} and R_{B2} at the [B] sites can be rewritten as

$$R_{A1} = \frac{P(Ti^{3+})}{P(Fe^{3+})} = \frac{V(Fe^{3+})}{V(Ti^{3+})}\exp\left\{10.24d_{AO}\left[V(Fe^{3+})^{1/2} - c_v V(Ti^{3+})^{1/2}\right]\right\}, \quad (12)$$

$$R_{A2} = \frac{P(M^{3+})}{P(Fe^{3+})} = \frac{V(Fe^{3+})}{V(M^{3+})}\exp\left\{10.24d_{AO}\left[V(Fe^{3+})^{1/2} - V(M^{3+})^{1/2}\right]\right\}, \quad (13)$$

$$R_{A4} = \frac{P(Ti^{2+})}{P(Fe^{3+})} = \frac{V(Fe^{3+})}{V(Ti^{2+})}\exp\left\{10.24\left[d_{AO}V(Fe^{3+})^{1/2} - d_{AO}c_v V(Ti^{2+})^{1/2} - d_{AB}V_{BA}(Ti^{2+})^{1/2}\right]\right\}, \quad (14)$$

$$R_{A5} = \frac{P(M^{2+})}{P(Fe^{3+})} = \frac{V(Fe^{3+})}{V(M^{2+})}\exp\left\{10.24\left[d_{AO}V(Fe^{3+})^{1/2} - d_{AO}V(M^{2+})^{1/2} - d_{AB}V_{BA}(M^{2+})^{1/2}\right]\right\}, \quad (15)$$

$$R_{A6} = \frac{P(Fe^{2+})}{P(Fe^{3+})} = \frac{V(Fe^{3+})}{V(Fe^{2+})}\exp\left\{10.24\left[d_{AO}V(Fe^{3+})^{1/2} - d_{AO}V(Fe^{2+})^{1/2} - d_{AB}V_{BA}(Fe^{2+})^{1/2}\right]\right\}, \quad (16)$$

$$R_{B1} = \frac{P(Ti^{3+})}{P(Fe^{3+})} = \frac{V(Fe^{3+})}{V(Ti^{3+})}\exp\left\{10.24d_{BO}\left[V(Fe^{3+})^{1/2} - c_v V(Ti^{3+})^{1/2}\right]\right\}, \quad (17)$$

$$R_{B2} = \frac{P(M^{3+})}{P(Fe^{3+})} = \frac{V(Fe^{3+})}{V(M^{3+})}\exp\left\{10.24d_{BO}\left[V(Fe^{3+})^{1/2} - V(M^{3+})^{1/2}\right]\right\}, \quad (18)$$

where M = Co or Mn; and $V(M^{2+})$, $V(M^{3+})$, $V(Ti^{2+})$, $V(Ti^{3+})$, $V(Fe^{2+})$, and $V(Fe^{3+})$ are the second and third ionization energies of Co, Mn, Ti, and Fe, respectively, as shown in Table 3. The parameter c_v is a barrier shape-correcting constant related to the potential barrier of Ti^{2+} and Ti^{3+} cations; we assume that c_v = 1.0 for other cations because the second and third ionization

 This journal is © The Royal Society of Chemistry 2018

Open Access Article. Published on 02 January 2018. Downloaded on 5/23/2026 9:34:01 PM.
This article is licensed under a Creative Commons Attribution 3.0 Unported Licence.

energies of Ti cations are distinctly lower than those of other cations. $V_{BA}(M^{2+})$, $V_{BA}(Ti^{2+})$, and $V_{BA}(Fe^{2+})$ are the heights of the equivalent potential barriers (all have a width of d_{AB}), which must be transmitted through by the M^{2+}, Ti^{2+}, and Fe^{2+} ions as they move from the [B] sites to the (A) sites during thermal treatment. The values of, d_{AO}, d_{BO}, and d_{AB} are the observed values in the XRD patterns, as listed in Table 1.

According to the O 2p itinerant-electron model, the magnetic moments of the Mn^{3+}, Ti^{2+}, and Ti^{3+} cations are antiparallel to those of Co^{2+}, Co^{3+}, Mn^{2+}, Fe^{3+}, and Fe^{2+} cations in the same sublattice of a spinel ferrite (see Table 3). Therefore, we can calculate the average magnetic moment per formula unit of a sample from eqn (4):

$$\left.\begin{aligned}
&\mu_C = \mu_{BT} - \mu_{AT},\\
&\mu_{AT} = -y_1 + m_3y_2 + 5y_3 - 2y_4 + m_2y_5 + 4y_6,\\
&\mu_{B1} = -2(x_1 - y_1 - y_4 - z_1) - z_1,\\
&\mu_{B2} = m_2(x_2 - y_2 - y_5 - z_2) + m_3z_2,\\
&\mu_{B3} = 4(3 - x_1 - x_2 - y_3 - y_6 - z_3) + 5z_3,\\
&\mu_{BT} = \mu_{B1} + \mu_{B2} + \mu_{B3},
\end{aligned}\right\}, \quad (19)$$

where μ_C is the calculated magnetic moment of a sample; μ_{AT} and μ_{BT} are the magnetic moments of the (A) and [B] sublattices; and μ_{B1}, μ_{B2}, and μ_{B3} are magnetic moments contributed by the Ti, Co (or Mn), and Fe ions, respectively, at the [B] sublattice.

For each sample, there are 22 parameters: y_1–y_6; z_1–z_3; N_3; R_{A1}, R_{A2}, R_{A4}, R_{A5}, and R_{A6}; R_{B1} and R_{B2}; $V_{BA}(Ti^{2+})$, $V_{BA}(M^{2+})$, and $V_{BA}(Fe^{2+})$; μ_C; and c_v. Altogether, there are 20 independent equations, including eqn (2), (3), (5)–(9), and (12)–(19), where eqn (8) contains five equations and eqn (9) contains two equations. Therefore, we needed to obtain the values of at least two independent parameters, such as c_v and $V_{BA}(Ti^{2+})$, in order to fit the observed values of μ_{exp} of a sample at 10 K.

Using the above parameters and equations, we fitted the dependence of μ_{exp} on x for the two series of samples. The points and curves in Fig. 5 represent the observed and

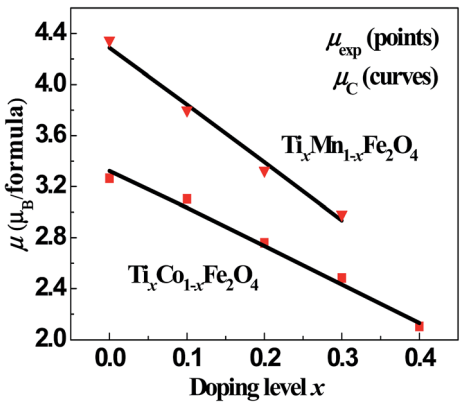

Fig. 5 Fitted magnetic moments, μ_C (line), and observed values, μ_{exp} (points), as functions of x for the two series of samples.

Table 4 Cation distributions obtained by fitting the dependence of the magnetic moments in the samples $Ti_xCo_{1-x}Fe_2O_4$ on x. The parameters $V_{BA}(Ti^{2+})$, $V_{BA}(Co^{2+})$, and $V_{BA}(Fe^{2+})$ are the heights of the potential barriers that must be transmitted though by the Ti^{2+}, Co^{2+}, and Fe^{2+} ions when moving from the [B] sites to the (A) sites during thermal treatment of the samples; N_3 is the total average number of trivalent cations per formula unit; μ_{AT} and μ_{BT} are the magnetic moments per formula unit of the (A) and [B] sublattices, respectively; and $\mu_C = \mu_{BT} - \mu_{AT}$ is the calculated magnetic moment per formula unit

x	0.0	0.1	0.2	0.3	0.4
N_3	0.9070	0.9496	0.9906	1.0297	1.0675
$V_{BA}(Ti^{2+})$ (eV)	1.0933	1.2900	1.4867	1.6833	1.8800
$V_{BA}(Co^{2+})$ (eV)	1.1542	1.3618	1.5694	1.7770	1.9847
$V_{BA}(Fe^{2+})$ (eV)	1.1056	1.3045	1.5034	1.7022	1.9011
A sites					
Ti^{3+}	0.0000	0.0168	0.0372	0.0602	0.0849
Co^{3+}	0.1164	0.1193	0.1172	0.1106	0.1002
Fe^{3+}	0.4159	0.4822	0.5392	0.5864	0.6244
Ti^{2+}	0.0000	0.0178	0.0283	0.0332	0.0343
Co^{2+}	0.1286	0.0919	0.0637	0.0429	0.0280
Fe^{2+}	0.3392	0.2706	0.2121	0.1639	0.1252
B sites					
Ti^{2+}	0.0000	0.0578	0.1202	0.1859	0.2536
Co^{2+}	0.6674	0.6173	0.5610	0.4992	0.4331
Fe^{2+}	0.9578	0.9935	1.0219	1.0424	1.0553
Ti^{3+}	0.0000	0.0091	0.0165	0.0228	0.0289
Co^{3+}	0.0931	0.0739	0.0586	0.0468	0.0377
Fe^{3+}	0.2816	0.2483	0.2219	0.2029	0.1914
μ_{BT} (μ_B per formula)	7.6142	7.2385	6.8574	6.4745	6.0925
μ_{AT} (μ_B per formula)	4.2909	4.2040	4.1225	4.0427	3.9621
μ_C (μ_B per formula)	3.3233	3.0345	2.7349	2.4318	2.1303

Table 5 Cation distributions obtained by fitting the dependence of the magnetic moments in the samples $Ti_xMn_{1-x}Fe_2O_4$ on x. The parameters $V_{BA}(Ti^{2+})$, $V_{BA}(Mn^{2+})$, and $V_{BA}(Fe^{2+})$ are the heights of the potential barriers that must be transmitted though by the Ti^{2+}, Mn^{2+}, and Fe^{2+} ions when moving from the [B] sites to the (A) sites during thermal treatment of the samples; N_3 is the total average number of trivalent cations per formula unit; μ_{AT} and μ_{BT} are the magnetic moments per formula unit of the (A) and [B] sublattices, respectively; and $\mu_C = \mu_{BT} - \mu_{AT}$ is the calculated magnetic moment per formula unit

x	0.0	0.1	0.2	0.3
N_3	0.8994	0.9373	0.9753	1.0132
$V_{BA}(Ti^{2+})$ (eV)	0.8960	1.0200	1.0800	1.1400
$V_{BA}(Mn^{2+})$ (eV)	1.1348	1.2057	1.2766	1.3476
$V_{BA}(Fe^{2+})$ (eV)	0.9708	1.0315	1.0921	1.1528
A sites				
Ti^{3+}	0.0000	0.0042	0.0090	0.0145
Mn^{3+}	0.0872	0.0847	0.0808	0.0755
Fe^{3+}	0.3319	0.3579	0.3840	0.4101
Ti^{2+}	0.0000	0.0104	0.0200	0.0290
Mn^{2+}	0.1789	0.1543	0.1312	0.1097
Fe^{2+}	0.4019	0.3885	0.3749	0.3612
B sites				
Ti^{2+}	0.0000	0.0795	0.1585	0.2371
Mn^{2+}	0.6225	0.5566	0.4911	0.4262
Fe^{2+}	0.8972	0.8734	0.8489	0.8235
Ti^{3+}	0.0000	0.0059	0.0124	0.0194
Mn^{3+}	0.1114	0.1044	0.0969	0.0885
Fe^{3+}	0.3689	0.3802	0.3922	0.4052
μ_{BT} (μ_B per formula)	8.1005	7.5945	7.0953	6.6036
μ_{AT} (μ_B per formula)	3.8129	3.7513	3.7033	3.6690
μ_C (μ_B per formula)	4.2876	3.8433	3.3921	2.9347

Open Access Article. Published on 02 January 2018. Downloaded on 5/23/2026 9:34:01 PM.
This article is licensed under a Creative Commons Attribution 3.0 Unported Licence.

calculated magnetic moments, μ_{exp} and μ_C, of the samples. It can be seen that the fitted curves are very close to the experimental results. In the fitting process, we obtained the cation distribution and other data, as listed in Tables 4 and 5. The cation distribution is shown as a function of x for the two series of samples in Fig. 6 and 7.

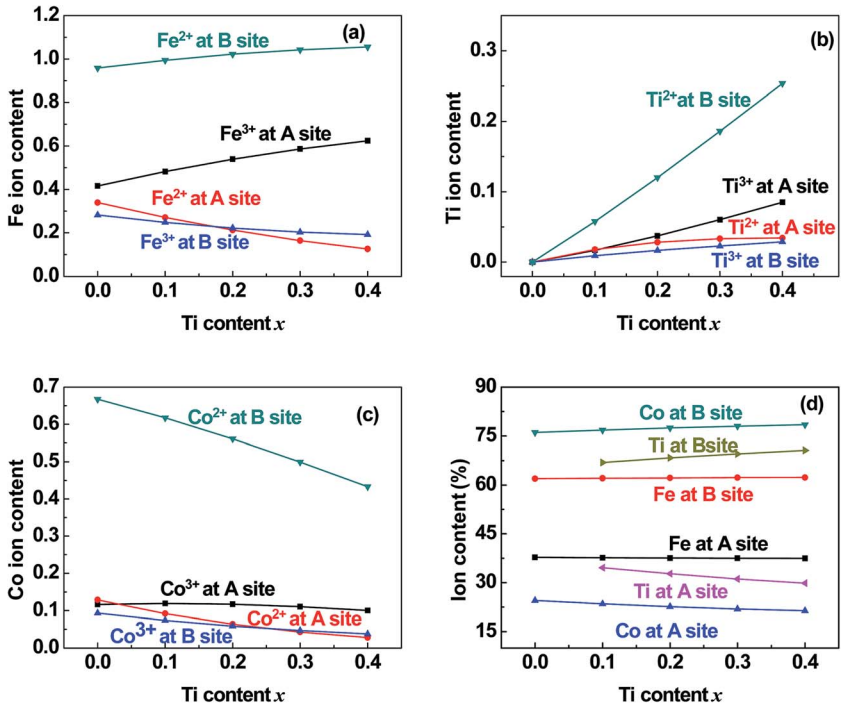

Fig. 6 Distribution of (a) Fe, (b) Ti, and (c) Co cations and (d) the total content percentages of different valence cations at the (A) and [B] sites in samples of $Ti_xCo_{1-x}Fe_2O_4$ ($0.0 \leq x \leq 0.4$).

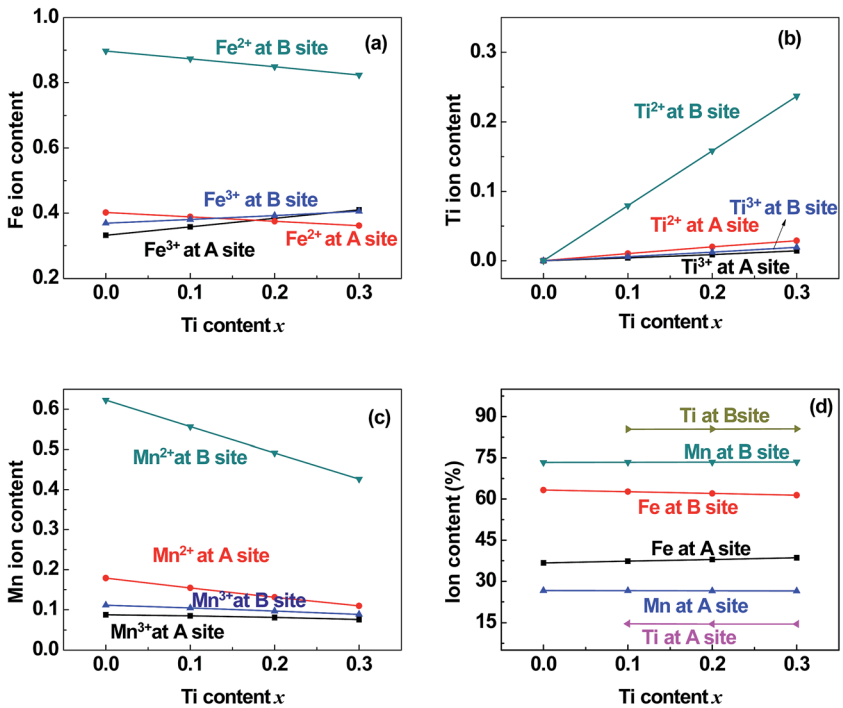

Fig. 7 Distribution of (a) Fe, (b) Ti, and (c) Mn cations and (d) the total content percentages of different valence cations at the (A) and [B] sites in samples of $Ti_xMn_{1-x}Fe_2O_4$ ($0.0 \leq x \leq 0.3$).

 This journal is © The Royal Society of Chemistry 2018

Open Access Article. Published on 02 January 2018. Downloaded on 5/23/2026 9:34:01 PM.
This article is licensed under a Creative Commons Attribution 3.0 Unported Licence.

5 Discussion

From Tables 4, 5, Fig. 6 and 7, we found that the fitting parameters and the cation distribution in the samples had certain characteristics, as discussed in the following subsections.

5.1 Fitting parameters: c_v and V_{BA}

During the fitting process, we determined that the potential barrier shape-correcting constant c_v was equal to 1.1 and 1.2 for the pair of ions, Ti–O, in the Co-series and Mn-series, respectively. Both values are reasonable when compared with $c_v = 1.0$ for other cation–anion pairs.

The Ti^{2+} ions must transmit though the equivalent potential barrier $V_{BA}(Ti^{2+})$ as they moved from the [B] sites to the (A) sites during the thermal treatment. We obtained the values of $V_{BA}(Ti^{2+})$ in the fitting process, and they increased from 1.093 eV ($x = 0.0$) to 1.880 eV ($x = 0.4$) for the Co-series and from 0.896 eV ($x = 0.0$) to 1.140 eV ($x = 0.3$) for the Mn-series. The values of $V_{BA}(Fe^{2+})$, $V_{BA}(Co^{2+})$, and $V_{BA}(Mn^{2+})$ were calculated from eqn (2) and (3), and they appear reasonable in the context of a physics problem.

5.2 Valence and distribution of Ti cations

(i) The ratio of Ti^{2+} ions at the (A) and [B] sites to the Ti-doping level, x, is more than 72% in the Co-series samples (Fig. 6(b)) and about 89% in the Mn-series samples (Fig. 7(b)). This result is similar to that measured using XPS and reported by Dupin *et al.*; they found that the average O ionic valence is −1.15 for TiO_2, which suggests that 70% of Ti cations in TiO_2 are Ti^{2+} ions.[26] Therefore, the conventional view[12–16] that all Ti cations in an oxide are Ti^{4+} ions needs to be modified.

(ii) The ratio of Ti^{2+} cations that entered the [B] sites to x increased from 58% ($x = 0.1$) to 63% ($x = 0.4$) in the Co-series samples (Fig. 6(b)), and this ratio remained at 79% from $x = 0.1$ to $x = 0.3$ in the Mn-series samples (Fig. 7(b)). This result is similar to that reported by Xu *et al.*, who found the ratio of Ti^{2+} cations that entered the [B] sites to x was 81% in Ti-doped ferrite $Ni_{0.68}Fe_{2.32}O_4$.[18]

(iii) The ratio of Ti cations, including Ti^{2+} and Ti^{3+}, that entered the [B] sites to x increased from 67% ($x = 0.1$) to 72% ($x = 0.4$) in the Co-series samples (Fig. 6(d)), and this ratio was 85% in the Mn-series samples (Fig. 7(d)). This result appears to be a balance between the contrasting results reported by several authors:[12–16] Kale *et al.* concluded that 71% of Ti cations entered the (A) sites in $Ti_{0.7}Ni_{1.7}Fe_{0.6}O_4$,[16] while other authors assumed that all of the Ti ions entered the [B] sites of the spinel ferrite samples.[12–15]

5.3 Distribution of Co cations in Co-series

(i) The ratio of Co cations, including Co^{2+} and Co^{3+}, that entered the [B] sites to the total Co cation content ranged from 76% to 78% (Fig. 6(d)). This ratio is very close to that reported by Shang *et al.*[30] for $Co_{1-x}Cr_xFe_2O_4$. This result is also close to that reported by Wakabayashi *et al.* for a $CoFe_2O_4$ film with thickness of 11 nm, which was based on soft X-ray absorption spectroscopy (XAS) and X-ray magnetic circular dichroism (XMCD) combined with cluster model calculations.[38]

(ii) The ratio of Co^{2+} cations that entered the [B] sites to the total Co cation content increased from 67% ($x = 0.0$) to 73% ($x = 0.4$). This result is similar to that reported by Shang *et al.*, who found that the ratio of Co^{2+} cations that entered the [B] sites ranged from 64% ($x = 0.0$) to 59% ($x = 0.8$) in $Co_{1-x}Cr_xFe_2O_4$.[30]

5.4 Distribution of Mn cations in Mn-series

The ratio of Mn^{2+} cations that entered the [B] sites to the total Mn cation content was 61%. The ratio of Mn ions, including Mn^{2+} and Mn^{3+} cations, that entered the [B] sites to the total Mn cation content was 73%. This result is similar to that reported by Xu *et al.*[20]

5.5 Entry of few Co and Mn cations into the (A) sites

It can be seen from Fig. 6(c) and 7(c) that a few of the Co (Mn) cations entered the (A) sites of the Co (Mn) series samples. This is in accordance with the observed results from XRD mentioned in Section 3.1: the ratio of observed to ideal values of A–O distance for $MnFe_2O_4$, 1.09, is higher than that for $CoFe_2O_4$, 1.04, because the effective radius of Mn is greater than that of Co (see Table 3). This suggested that a few of the Mn (Co) cations entered the (A) sites of $MnFe_2O_4$ ($CoFe_2O_4$).

6 Conclusions

The single-phase spinel ferrites $Ti_xCo_{1-x}Fe_2O_4$ ($0.0 \le x \le 0.4$) and $Ti_xMn_{1-x}Fe_2O_4$ ($0.0 \le x \le 0.3$) were prepared using the conventional method for preparing ceramics. The samples were found to consist of a single phase with a cubic spinel structure. The lattice constant increased in the Co-series samples and decreased in the Mn-series samples with increases in the dopant level, x. The values of μ_{exp} of the two series of samples, measured at 10 K, decreased approximate linearly with increasing x.

The dependence of μ_{exp} on x for the two series of samples was fitted using a quantum-mechanical potential barrier method. The fitted magnetic moments were very close to the experimental results. In the fitting process, the cation distributions of the two series of samples were obtained.

The cation distributions and the magnetic structure obtained in this study are distinctly different from those reported by other groups: (i) there were Ti^{2+} and Ti^{3+} ions, but no Ti^{4+} ions, in our samples. (ii) The ratio of Ti^{2+} cations that entered the [B] sites to the Ti-doping level, x, increased from 58% ($x = 0.1$) to 63% ($x = 0.4$) in the Co-series samples, and this ratio was 79% from $x = 0.1$ to $x = 0.3$ in the Mn-series samples. (iii) The magnetic moments of Ti^{2+}, Ti^{3+}, and Mn^{3+} ions (with 3d electron number of $n_d \le 4$) coupled antiferromagnetically with other cations ($n_d \ge 5$) whenever they were at the (A) or [B] sublattice.

Open Access Article. Published on 02 January 2018. Downloaded on 5/23/2026 9:34:01 PM.
This article is licensed under a Creative Commons Attribution 3.0 Unported Licence.

Conflicts of interest

There are no conflicts to declare.

Acknowledgements

This work is supported by the National Natural Science Foundation of China (NSF-11174069), the Natural Science Foundation of Hebei Province (A2015205111), the Key item Science Foundation of Hebei Province (Grant No. 16961106D), and the Young scholar Science Foundation of the Education Department of Hebei Province (QN2016015).

References

1 W. M. Xu, G. R. Hearne, S. Layek, D. Levy, J.-P. Itié, M. P. Pasternak, G. Kh. Rozenberg and E. Greenberg, *Phys. Rev. B: Condens. Matter Mater. Phys.*, 2017, **96**, 045108.
2 K. Ugendar, S. Samanta, S. Rayaprol, V. Siruguri, G. Markandeyulu and B. R. K. Nanda, *Phys. Rev. B: Condens. Matter Mater. Phys.*, 2017, **96**, 035138.
3 O. Kuschel, R. Buß, W. Spiess, T. Schemme, J. Wollermann, K. Balinski, A. T. N'Diaye, T. Kuschel, J. Wollschlager and K. Kuepper, *Phys. Rev. B: Condens. Matter Mater. Phys.*, 2016, **94**, 094423.
4 G. Lavorato, E. Winkler, B. Rivas-Murias and F. Rivadulla, *Phys. Rev. B: Condens. Matter Mater. Phys.*, 2016, **94**, 054405.
5 M. Abes, C. T. Koops, S. B. Hrkac, J. McCord, N. O. Urs, N. Wolff, L. Kienle, W. J. Ren, L. Bouchenoire, B. M. Murphy and O. M. Magnussen, *Phys. Rev. B: Condens. Matter Mater. Phys.*, 2016, **93**, 195427.
6 T. Watanabe, S. Takita, K. Tomiyasu and K. Kamazawa, *Phys. Rev. B: Condens. Matter Mater. Phys.*, 2015, **92**, 174420.
7 D. Fritsch and C. Ederer, *Phys. Rev. B: Condens. Matter Mater. Phys.*, 2012, **86**, 014406.
8 D. Venkateshvaran, M. Althammer, A. Nielsen, S. Geprägs, M. S. Ramachandra Rao, S. T. B. Goennenwein, M. Opel and R. Gross, *Phys. Rev. B: Condens. Matter Mater. Phys.*, 2009, **79**, 134405.
9 M. Reehuis, M. Tovar, D. M. Többens, P. Pattison, A. Hoser and B. Lake, *Phys. Rev. B: Condens. Matter Mater. Phys.*, 2015, **91**, 024407.
10 C. W. Chen, *Magnetism and Metallurgy of Soft Magnetic Materials*, North-Holland Publishing Company, 1977, pp. 171–417.
11 J. M. D. Coey, *Magnetism and Magnetic Materials*, Cambridge University Press, 2010, pp. 414–427.
12 G. D. Dwivedi, A. G. Joshi, H. Kevin, P. Shahi, A. Kumar, A. K. Ghosh, H. D. Yang and S. Chatterjee, *Solid State Commun.*, 2012, **152**, 360–363.
13 K. Srinivasa Rao, A. Mahesh Kumar a, M. Chaitanya Varma, G. S. V. R. K. Choudary and K. H. Rao, *J. Alloys Compd.*, 2009, **488**, 6–9.
14 E. Schmidbauer, *Solid State Commun.*, 1976, **18**, 301–303.
15 E. Schmidbauer, *Phys. Chem. Miner.*, 1983, **9**, 124–126.
16 C. M. Kale, P. P. Bardapurkar, S. J. Shukla and K. M. Jadhav, *J. Magn. Magn. Mater.*, 2013, **331**, 220–224.
17 J. Xu, D. H. Ji, Z. Z. Li, W. H. Qi, G. D. Tang, Z. F. Shang and X. Y. Zhang, *J. Alloys Compd.*, 2015, **619**, 228–234.
18 J. Xu, D. H. Ji, Z. Z. Li, W. H. Qi, G. D. Tang, X. Y. Zhang, Z. F. Shang and L. L. Lang, *Phys. Status Solidi B*, 2015, **252**, 411–420.
19 J. Xu, W. H. Qi, D. H. Ji, Z. Z. Li, G. D. Tang, X. Y. Zhang, Z. F. Shang and L. L. Lang, *Acta Phys. Sin.*, 2015, **64**, 017501.
20 J. Xu, L. Ma, Z. Z. Li, L. L. Lang, W. H. Qi, G. D. Tang, L. Q. Wu, L. C. Xue and G. H. Wu, *Phys. Status Solidi B*, 2015, **252**, 2820–2829.
21 G. D. Tang, D. H. Ji, Y. X. Yao, S. P. Liu, Z. Z. Li, W. H. Qi, Q. J. Han, X. Hou and D. L. Hou, *Appl. Phys. Lett.*, 2011, **98**, 072511.
22 S. R. Liu, D. H. Ji, J. Xu, Z. Z. Li, G. D. Tang, R. R. Bian, W. H. Qi, Z. F. Shang and X. Y. Zhang, *J. Alloys Compd.*, 2013, **581**, 616–624.
23 R. E. Cohen, *Nature*, 1992, **358**, 136–138.
24 R. E. Cohen and H. Krakauer, *Phys. Rev. B: Condens. Matter Mater. Phys.*, 1990, **42**, 6416–6423.
25 L. Q. Wu, Y. C. Li, S. Q. Li, Z. Z. Li, G. D. Tang, W. H. Qi, L. C. Xue, X. S. Ge and L. L. Ding, *AIP Adv.*, 2015, **5**, 097210.
26 J. C. Dupin, D. Gonbeau, P. Vinatier and A. Levasseur, *Phys. Chem. Chem. Phys.*, 2000, **2**, 1319–1324.
27 D. H. Ji, G. D. Tang, Z. Z. Li, X. Hou, Q. J. Han, W. H. Qi, R. R. Bian and S. R. Liu, *J. Magn. Magn. Mater.*, 2013, **326**, 197–200.
28 G. D. Tang, Q. J. Han, J. Xu, D. H. Ji, W. H. Qi, Z. Z. Li, Z. F. Shang and X. Y. Zhang, *Phys. B*, 2014, **438**, 91–96.
29 L. L. Lang, J. Xu, W. H. Qi, Z. Z. Li, G. D. Tang, Z. F. Shang, X. Y. Zhang, L. Q. Wu and L. C. Xue, *J. Appl. Phys.*, 2014, **116**, 123901.
30 Z. F. Shang, W. H. Qi, D. H. Ji, J. Xu, G. D. Tang, X. Y. Zhang, Z. Z. Li and L. L. Lang, *Chin. Phys. B*, 2014, **23**, 107503.
31 X. Y. Zhang, J. Xu, Z. Z. Li, W. H. Qi, G. D. Tang, Z. F. Shang, D. H. Ji and L. L. Lang, *Phys. B*, 2014, **446**, 92–99.
32 L. L. Lang, J. Xu, Z. Z. Li, W. H. Qi, G. D. Tang, Z. F. Shang, X. Y. Zhang, L. Q. Wu and L. C. Xue, *Phys. B*, 2015, **462**, 47–53.
33 G. D. Tang, Z. F. Shang, X. Y. Zhang, J. Xu, Z. Z. Li, C. M. Zhen, W. H. Qi and L. L. Lang, *Phys. B*, 2015, **463**, 26–29.
34 L. C. Xue, L. L. Lang, J. Xu, Z. Z. Li, W. H. Qi, G. D. Tang and L. Q. Wu, *AIP Adv.*, 2015, **5**, 097167.
35 L. L. Ding, L. C. Xue, Z. Z. Li, S. Q. Li, G. D. Tang, W. H. Qi, L. Q. Wu and X. S. Ge, *AIP Adv.*, 2016, **6**, 105012.
36 H. M. Rietveld, *J. Appl. Crystallogr.*, 1969, **2**, 65–71.
37 R. D. Shannon, *Acta Crystallogr., Sect. A: Cryst. Phys., Diffr., Theor. Gen. Crystallogr.*, 1976, **32**, 751–767.
38 Y. K. Wakabayashi, Y. Nonaka, Y. Takeda, S. Sakamoto, K. Ikeda, Z. Chi, G. Shibata, A. Tanaka, Y. Saitoh, H. Yamagami, M. Tanaka, A. Fujimori and R. Nakane, *Phys. Rev. B: Condens. Matter Mater. Phys.*, 2017, **96**, 104410.

 This journal is © The Royal Society of Chemistry 2018